Transition metal co-precipitation mechanisms in silicon

T. Buonassisi [a,*], M. Heuer [a,1], A.A. Istratov [a,2], M.D. Pickett [a,3], M.A. Marcus [b], B. Lai [c], Z. Cai [c], S.M. Heald [c], E.R. Weber [a,4]

[a] *Department of Materials Science and Engineering, University of California, Berkeley and Materials Science Division, Lawrence Berkeley National Laboratory, Berkeley, CA 94720, USA*
[b] *Advanced Light Source, Lawrence Berkeley National Laboratory, Berkeley, CA 94720, USA*
[c] *Advanced Photon Source, Argonne National Laboratory, Argonne, IL 60439, USA*

Abstract

Formation mechanisms of precipitates containing multiple-metal species in silicon are elucidated by nano-scale morphology and phase investigations performed by synchrotron-based X-ray microprobe techniques. Precipitates formed at low (655 °C) and high (1200 °C+) temperatures exhibit distinguishing features indicative of unique formation mechanisms. After lower-temperature annealing, co-localized single-metal silicide phases are observed, consistent with classical models predicting that dissolved, supersaturated metal atoms will precipitate into solid second-phase particles. Precise precipitate morphologies are found to depend on the local crystallographic environment. In precipitates formed during slow cooling from higher-temperature anneals, nano-scale phase separation and intermetallic phases are evident, suggestive of a high-temperature transition through a liquid phase. Based on experimental results and phase diagram information, it is proposed that under certain conditions, liquid metal–silicon droplets may form within the silicon matrix, possibly with the potential to getter additional metal atoms via liquid–solid segregation.

Keywords: Defect engineering; Precipitation; Intermetallics; Multicrystalline silicon; Photovoltaics

1. Introduction

It is commonly accepted that stringent control over metal impurity distributions is key to achieving high performance silicon-based devices, e.g., integrated circuits and solar cells [1,2]. Effective control over metal distributions requires a thorough understanding of metal precipitation reactions, as these determine the concentration of metals remaining homogeneously dissolved in silicon as deleterious, lifetime-limiting point defects. For multicrystalline silicon (mc-Si), material out of which over 50% of solar cells worldwide are made, metal precipitation reactions are further complicated by the inhomogeneous presence of structural defects and the possible presence of up to 15 metallic impurity species in concentrations as high as 10^{12} cm^{-3} or greater [3–5].

It is also commonly accepted as well that interstitially dissolved 3d transition metals in silicon (e.g., iron or copper) can, upon supersaturation, precipitate into their solid equilibrium metal silicide phase (e.g., $FeSi_2$ [6] or Cu_3Si [7–9]). It is also fairly well established that the presence of precipitates of one metal species may aid the precipitation of another (see [10] and references therein), e.g., by providing energetically favorable nucleation sites via lattice strain or

* Corresponding author. Present address: Massachusetts Institute of Technology, Cambridge, MA 02139, USA. Tel.: +1 510 717 8413.
E-mail addresses: buonassisi@alumni.nd.edu, buonassisi@mac.com (T. Buonassisi).
[1] Present address: BerlinSolar GmbH, Magnusstrasse 11, 12489 Berlin, Germany.
[2] Present address: Siltronic Corporation, 7200 NW Front Avenue, M/S 10, Portland, OR 97210, USA.
[3] Present address: Hewlett-Packard Laboratories, Palo Alto, CA 94304, USA.
[4] Present address: Fraunhofer Institute for Solar Energy Systems, 79110 Freiburg, Germany.

local native point defect compensation. Indeed, microscopic investigations of metal distributions in mc-Si frequently reveal multiple metals precipitated at the same location [10–14]. Aside from speculative arguments on the basis of elemental co-localization, no experimental evidence had concluded that metals react chemically with each other in silicon during precipitation to form alloy compounds.

In parallel fields of research, it is commonly accepted that multiple metallic species can simultaneously form compounds with silicon. In metal alloys, mixed-metal silicide systems have been reported from the mundane Si–Fe–Cr–Ni [15] to the exotic Ti–Cu–Ni–Al–Zr–Si–B [16], among many others [17–21]. Those studying thin films of metal/metal silicide compounds on Si substrates also reported intermixing of metallic species, leading to the formation of solid solutions and ternary compounds (see Ref. [22] for a review). These metal–alloy and thin-film compounds typically form via the solidification of a mixed-element liquid, or via solid state diffusion of atoms in adjacent layers. The likelihood of each process is highly a function of the phase diagrams in question [22]; additional evidence for a particular reaction pathway is provided by the micro- or nano-scale phase morphology. Finally, in studies of metal point defects in silicon, new or absent deep-level transient spectroscopy peaks observed in Si contaminated with multiple-metal species have been attributed to M1–M2 pairs [23–25], and yet others have been predicted [25,26] through simulations.

Given these numerous developments in parallel fields, it is surprising that only in 2004 did synchrotron-based investigations conclusively demonstrate that different metal species can indeed react chemically within the silicon bulk, forming precipitates of new phases or solid solutions [27,28]. One such system was recently identified by Heuer et al. [29] as consisting of α-$NiSi_2$ with Cu and Fe as substitutional impurities. The presence of such systems challenges the traditional model of metal precipitation in silicon, and raises the possibility of more complex precipitation reaction mechanisms, e.g., solid state diffusion or involvement of an intermediate liquid phase.

This study uses sub-micron-focused synchrotron-based X-rays to probe the nano-structure and chemical states of multiple-metal precipitates formed under various reaction conditions in bulk Si. By analysis of the precipitate nanostructure, chemical state and temperature of formation, in combination with phase diagram information, mechanisms of multiple-metal co-precipitation in silicon are proposed.

2. Materials and methods

A set of silicon samples was carefully selected to achieve well-defined structural defect distributions with low background metal concentration. These materials include Czochralski silicon (CZ-Si) with a fairly uniform distribution of $1.8\times10^{6}\,cm^{-3}$ oxygen precipitates and B doping of $1.5\times10^{15}\,cm^{-3}$, and multicrystalline float zone (mc-FZ [30]) with a high density of structural defects such as dislocations and grain boundaries, grown at the National Renewable Energy Laboratory. Both CZ-Si and mc-FZ sample thicknesses were on the order of 700 μm.

Both types of model defect structure were cleaned using a light chemical etch, then intentionally contaminated by scratching with high-purity copper, nickel and iron wires; a drive-in anneal was then performed at 1200 °C for all samples. This high-temperature anneal determined the total concentration of metals within the samples, corresponding to Cu, Ni and Fe solubilities of 4.4×10^{18}, 2.2×10^{18} and 1.6×10^{16} atoms cm^{-3}, respectively. One subset of samples was quenched in silicone oil (to inhibit precipitate formation), etched to remove surface metals (which may act as efficient sinks for bulk-dissolved metals during the subsequent anneal), then inserted into a pre-heated furnace running at 655 °C, annealed for 2.5 h (to facilitate precipitate formation), and allowed to cool slowly to room temperature. The precipitate morphology and chemistry is largely determined by this low-temperature anneal. Below, these samples are referred to as 'lower-temperature annealing'. The other subset of samples was slowly cooled to room temperature from 1200 °C. These are referred to as 'higher-temperature annealing'.

To substantiate results obtained on 'higher-temperature annealing' intentionally contaminated model defect structures, as-grown mc-Si material was selected from near the bottom of an ingot, in a region known to contain Cu, Fe and Ni in bulk concentrations above $10^{14}\,cm^{-3}$ [3–5] and multiple-metal precipitates several tens of nanometers in diameter [3,31]. Ingot mc-Si sample thicknesses were on the order of 250 μm.

The surfaces of all samples were treated with a light chemical etching prior to synchrotron-based analyses, thus reducing the risk of measurement artifacts originating from surface contaminants.

X-ray fluorescence microscopy (μ-XRF) mapping was employed to determine the size and spatial distributions, as well as elemental composition and nano-/micro-scale morphologies, of individual metal impurity nano-precipitates (see Refs. [32,33] for details). Measurement geometry was selected for the sample normal, varying between approximately 15° and 45° relative to the incoming beam, and thus the information depth (i.e., thickness of material after which the XRF signal intensity decays to $1/e$, a strong function of the X-ray fluorescence energy [32]) varied between 9 and 25 μm for iron (K-edge fluorescence at 6.4 keV) and between 18 and 50 μm for copper (K-edge at 8 keV). This arrangement allows one to probe for metals well beneath the sample surface, while minimizing the risk of artifacts caused by inadvertent residual contamination on the sample back surfaces.

Once a metal impurity precipitate of interest was located, X-ray absorption microspectroscopy (μ-XAS) was performed on the regions with distinct elemental

composition to determine the local chemical state (see [32,33] for details). The absorption spectra allow one to determine what chemical interactions, if any, exist between individual elemental species at a given location within a metal-rich precipitate. For truly nanometer-scale precipitates, a full absorption spectrum was often not possible because of signal-to-noise and beamline optics limitations. In these cases, only the portion of the X-ray absorption spectrum close to the absorption edge was obtained, a sub-technique of μ-XAS known as μ-XANES (X-ray absorption near-edge microspectroscopy; see Refs. [6,9] for examples).

Beamline 2-ID-D [34] at the Advanced Photon Source (APS) at Argonne National Laboratory was utilized for sub-micron-focused μ-XRF and μ-XANES. At this beamline, zone-plate lenses can regularly achieve a focused spot size on the order of 200 nm. High-resolution μ-XRF linescans were obtained at this beamline, with positional (XY stage) accuracy of ~20 nm, and count rate accuracies within 5%. Error bars are barely visible on the scale of the diagrams as presented, and are hence omitted. Additionally, beamlines 20-ID-B [35] of the APS and 10.3.2 [36] at the Advanced Light Source at Lawrence Berkeley National Laboratory were employed for micron-scale μ-XRF and full μ-XAS.

3. Results

3.1. Precipitates formed as result of lower-temperature annealing (655 °C)

A high degree of metal supersaturation results in a high density of metal-rich precipitates after the 655 °C precipitate ripening anneal. In CZ-Si, a high density of metal-rich precipitates is observed in the single-crystalline regions between oxygen precipitates, as shown in Fig. 1a and b. A closer examination of this sample produces several noteworthy observations. First, although metal precipitates appear predominantly co-localized (e.g., Cu-rich and Ni-rich precipitates form at approximately the same locations, Fig. 1a–d), only equilibrium single-metal silicide phases are detected (Cu_3Si, shown in Fig. 1e, and $NiSi_2$, not shown). Secondly, the Cu_3Si clusters shown in Fig 1a tend to align along certain crystallographic planes within the single-crystalline matrix. Thirdly, a low Cu count rate within each Cu-rich cluster (Fig. 1c) suggests that Cu_3Si is present as a haze (colony) of nano-precipitates, as opposed to a large continuous particle. Furthermore, this Cu_3Si haze appears to encircle discrete $NiSi_2$ particles, as might be expected given the well-known Cu_3Si nano-precipitate colony formation mechanism discussed in Section 4.1.

In the mc-FZ sample, most of the above observations apply (multiple-metal co-localization, single-metal silicide phases), as evidenced in Fig. 2. It is worth noting the considerably higher density of particles observed along the grain boundary, a structural defect that offers abundant heterogeneous nucleation sites.

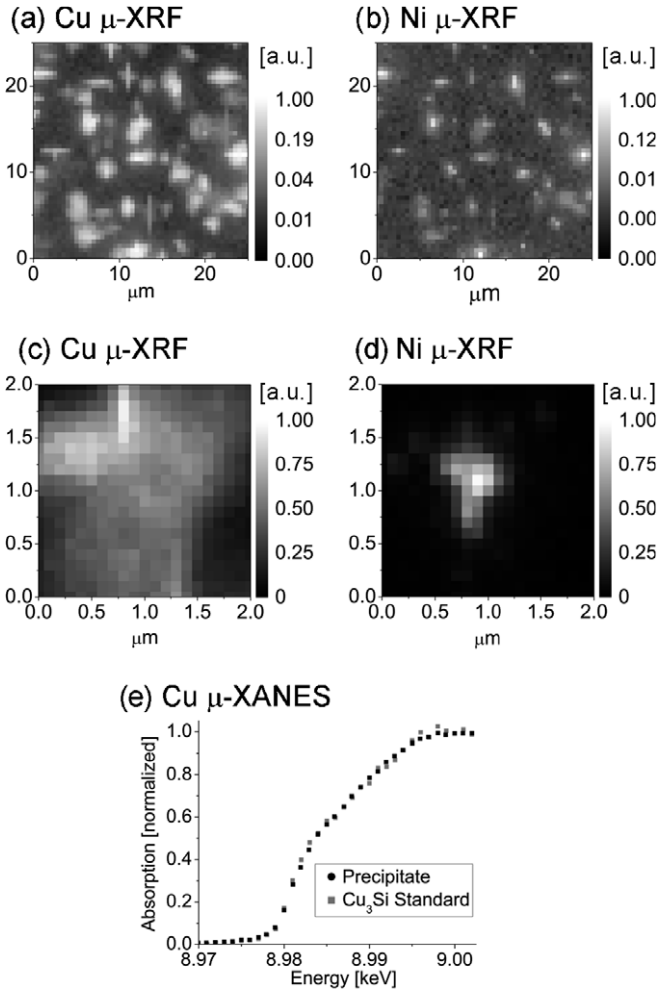

Fig. 1. (a,b) Cu and Ni precipitates in single-crystalline silicon after a quench from 1200 °C and a subsequent anneal at 655 °C. Note the co-localization of Cu- and Ni-rich particles, and the preference for Cu-rich precipitates to lie along certain crystallographic orientations. (c,d) High-resolution map of a single metal-rich cluster. While the Ni-rich particle is spatially localized, the Cu-rich cluster is diffuse with a low average XRF count rate, indicating a colony of nano-precipitates. (e) μ-XANES indicates the chemical states of these particles are single-metal silicides (e.g., Cu_3Si), with no detectable chemical mixing between different metal species.

3.2. Precipitates formed as result of higher-temperature annealing (1200 °C) and crystal growth (1414 °C)

In intentionally contaminated CZ-Si and mc-FZ samples slowly cooled from higher temperatures, a low density of large precipitates is observed. In these precipitates, co-localization of various elemental species is again evident, as seen in Fig. 3a–c. A high XRF count rate is evidence for solid, or near-solid, precipitates, as opposed to a haze (colony) of nano-precipitates.

Nano-scale phase separation is observed in these precipitates. While the multiple-metal-rich precipitate core (indicated as α in Fig. 3c and d) consists of co-localized Fe, Ni, Cu and a trace of Cr (Fig. 3i), a small Cu-rich nodule is observed adjacent (β in Fig. 3c and d). μ-XANES measure-

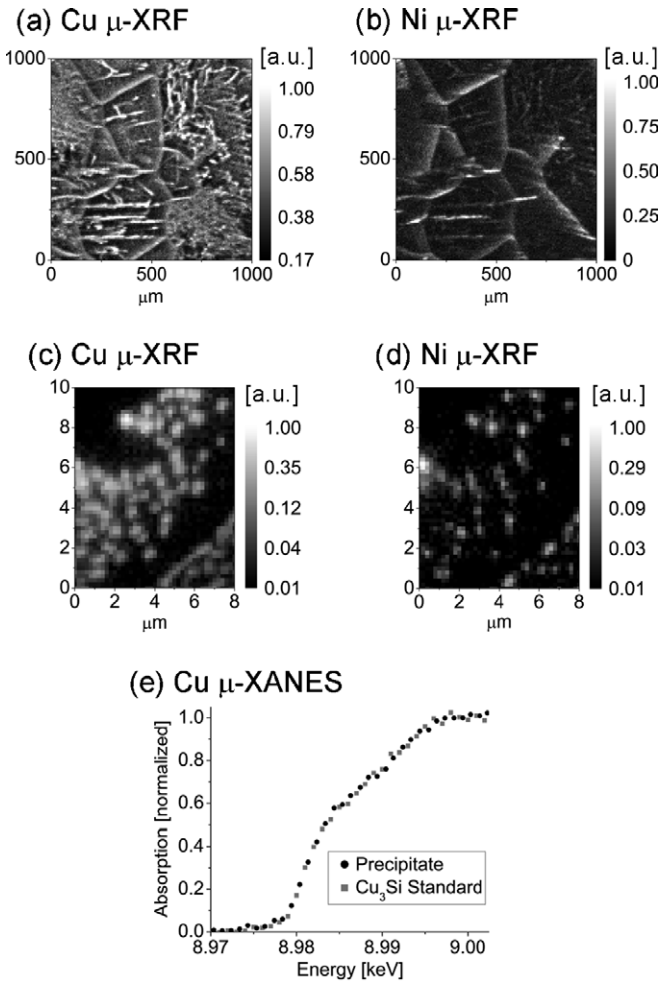

Fig. 2. (a,b) Cu and Ni precipitates in mc-FZ silicon after a quench from 1200 °C and a subsequent anneal at 655 °C. Note the co-localization of Cu- and Ni-rich particles along certain grain boundaries. (c,d) High-resolution map of metal-rich clusters along a grain boundary observed in projection, with the decay of signal intensity from the near surface (left) into the bulk (right). Note that both Cu and Ni form high densities of particles along the grain boundary, as opposed to isolated colonies of nano-precipitates (Fig. 1). (e) XANES on precipitates in quenched mc-FZ indicates these particles are single-metal silicides, with no detectable chemical mixing.

ments of the multiple-metal-rich core (α, Fig. 3e) reveal that different elements at this location are chemically bonded to each other. By comparison with standard references, it is apparent that Cu is a substitutional impurity within a α-$NiSi_2$ host structure, forming a system akin to that described in Ref. [29] and illustrated in Fig. 3g. Conversely, XANES measurements of the Cu-rich nodule (β, Fig. 3f) reveal Cu in a Cu_3Si phase, illustrated in Fig. 3h.

These results are largely substantiated by observations of Cu + Fe + Ni-rich particles in as-grown ingot mc-Si (Fig. 4). Similar nano-scale phase separation is observed in these samples (Fig. 4c and d). Because the metal-rich cluster was smaller than the beam spot size (200 nm), it was not possible to take XANES measurements at both the multiple-metal-rich core (α) and the Cu-rich nodule (β). A XANES measurement taken on β reveals that the

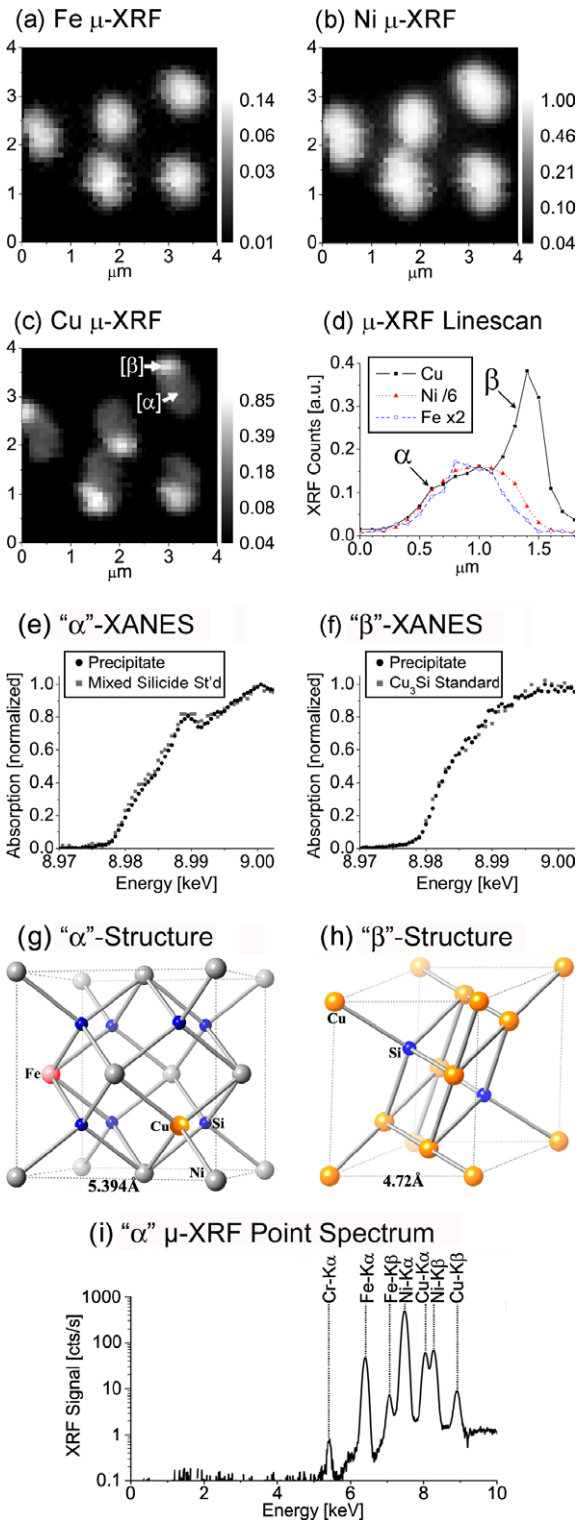

Fig. 3. (a–c) High-resolution map of Fe, Ni and Cu distributions in a multiple-metal-rich cluster in a sample slowly cooled from 1200 °C. (d) Linescan across one of the metal-rich clusters indicates speciation of the Cu into two distinct regions, denoted by α and β. While α consists of multiple metals, β is primarily Cu. (e,g) Cu-XANES indicates that the Cu in α is a substitutional impurity in the $NiSi_2$ structure, revealing chemical mixing of different elements. (f,h) Cu-XANES indicates Cu in β is in a Cu_3Si phase (η'-Cu_3Si structure shown). (i) Background-subtracted μ-XRF point spectrum of α, indicating the presence of Ni, Fe, Cu and a trace of Cr.

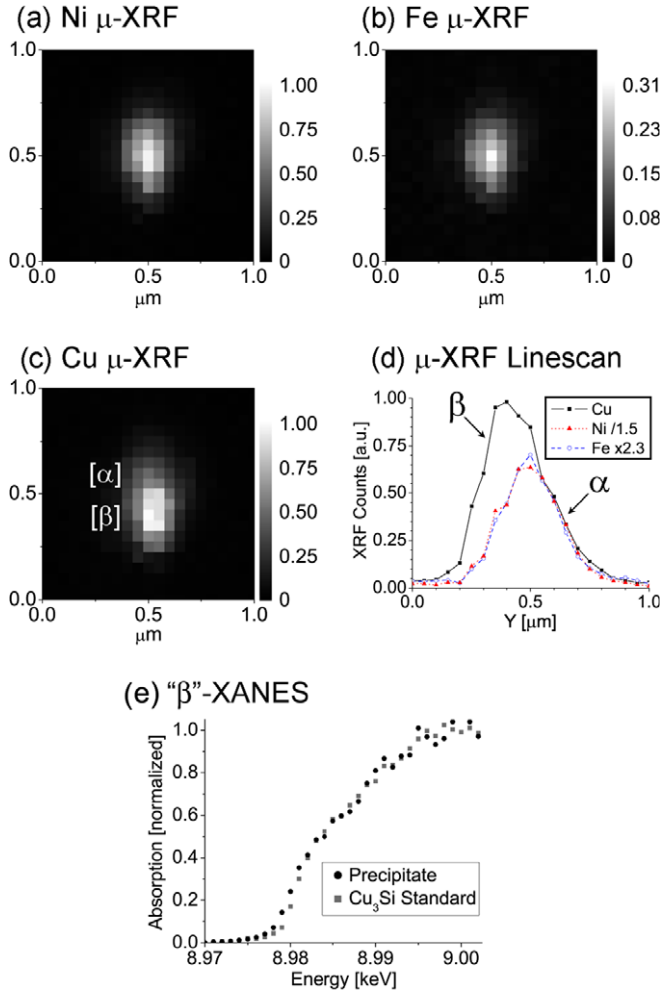

Fig. 4. (a–c) High-resolution map of Ni, Fe and Cu distributions in a multiple-metal-rich cluster in a silicon sample cut from near the bottom of an as-grown mc-Si ingot. (d) μ-XRF linescan in the vertical dimension across the metal-rich cluster indicates speciation of the Cu into two distinct regions, denoted by α and β. While α consists of multiple metals, β is primarily Cu. (e) Cu-XANES on β indicates that Cu is predominantly in the Cu_3Si phase. Cu-XANES on pure α was not possible due to the comparatively large beam spot size (200 nm) and low Cu concentration.

majority of Cu is in the Cu_3Si chemical state; unfortunately, measurements on the multiple-metal-rich core α were not possible, owing to the comparatively large beam spot size (200 nm) and low local Cu concentrations.

4. Discussion

4.1. Precipitates formed as result of lower-temperature annealing (655 °C)

Features of precipitates formed via lower-temperature annealing can be comprehensively explained using classical precipitation models. First, the chemical states of all measured precipitates are equilibrium (silicon-rich) single-metal silicides (e.g., $NiSi_2$, Cu_3Si), in agreement with established thermodynamics [9,37]. No mixed-metal silicide systems were observed. Secondly, precipitate nucleation and growth appears to be facilitated by strain minimization and the presence of defects or other metal precipitates. This is evidenced by the high degree of coincidence between metal silicide precipitates and structural defects, as well as the co-localization of metal silicide precipitates of different species, as shown in Fig. 1 (note the Cu_3Si colony surrounding the $NiSi_2$ precipitate). Precipitate or microcolony growth along preferred crystallographic planes, evidenced in Fig. 1, is yet another manifestation of interface strain minimization.

Lastly, the presence of comparatively large Cu_3Si microcolonies in single-crystalline silicon with heterogeneous nucleation sites, shown in Fig. 1, is consistent with existing models [8,38] describing nano-precipitate colony formation via repeated Cu_3Si nucleation on climbing dislocations. However, compared with the large colonies shown in Fig. 1 a and b, the particles observed along grain boundaries in mc-FZ are smaller by at least a factor of five, as shown in Fig. 2c and d. From this one may conclude that the heterogeneous nucleation site microstructure has an obvious impact on precipitate formation; perhaps it is more energetically favorable for Cu to diffuse along these grain boundaries to the next available nucleation site rather than form micron-sized nano-precipitate colonies into the single-crystalline grains, and/or perhaps colonies of nano-precipitates are present but in much smaller sizes.

In closing, metal precipitation into solid, equilibrium single-metal silicide phases, facilitated by lattice strain minimization or by the presence of defects/other metal precipitates/favorable point defect concentrations, and Cu_3Si microcolony growth (in single-crystalline silicon), are all well explained by existing precipitation models and thermodynamic understanding.

4.2. Precipitates formed as result of higher-temperature annealing (1200 °C) and crystal growth (1414 °C)

Certain features evident in these precipitates are difficult to explain using classic precipitation models and invite the postulation of other, alternative precipitation mechanisms. For instance, the formation of mixed-metal silicide systems (e.g., Fig. 3) suggests that these precipitates formed either via a liquid–alloy intermediate phase, via precipitation of several co-located dissolved impurity species into a mixed-metal silicide particle, or via solid state diffusion of atoms between adjacent but distinct metal silicide phases. While all three mechanisms may be possible given the appropriate reaction conditions, the first possibility appears to be more likely for the particular samples under discussion, given the observed nano-scale phase separation, relatively repeatable and homogeneous compositions, and large precipitate sizes, in addition to respective metal–silicon phase diagram information. Experimental evidence and rationale leading to this conclusion is described below.

A review of binary phase diagrams indicates that, in most eutectic systems, the point of maximum solid solubility of an arbitrary element *A* dissolved within a solid matrix

of element B occurs at the A–B eutectic temperature. However, when the enthalpy of formation of an A point defect within a B matrix is large, as is the case of 3d transition metal point defects in silicon, the point of maximum solid solubility can occur at temperatures several hundreds of degrees above the eutectic. This phenomenon, known as retrograde solubility, affects several dissolved 3d transition metal elements in silicon, including Cu, Ni and Fe [39]. Consequently, the onset of metal supersaturation in the samples herein discussed occurs at temperatures well above the eutectic temperatures of Ni–Si (966 °C, Fig. 5) and Cu–Si (802 °C, Fig. 5), as demonstrated in Fig. 6a.

While precipitation with low M concentrations is expected to occur via the pathway presented in Fig. 6b, the shift of maximum solubility to temperatures higher than the eutectic temperature provides the theoretical possibility for certain metals in high concentrations to precipitate and form liquid-phase particles, as demonstrated by Fig. 6c. While in situ TEM measurements by Dahmen et al. [40] and Xu et al. [41] have observed the melting of pre-existing precipitates in other matrices (Pb precipitates in Al, and Ge precipitates in SiO_x, respectively), the observation of precipitation and growth of liquid metal clusters during cooling is much more challenging (supersaturated metals predominantly diffuse out to the TEM sample surfaces, which are typically less than 1 μm away).

Nano-scale phase separation, as evidenced by Figs. 3 and 4, is again consistent with phase speciation occurring during solidification of liquids with near-eutectic compositions. During cooling, the liquid system (droplet) may expel certain impurities as it follows the liquidus of the multiple-element phase diagram towards the eutectic point. Further phase separation can occur during solidification of a liquid of eutectic composition, as solid equilibrium silicide phases are seldom of the precise eutectic composition. The end result of liquid solidification is a repeatable structure of distinct phases. The patterns observed in Figs. 3 and 4 appear to be consistent with this model. Although the low Cu–Si eutectic temperature suggests that copper is likely to play

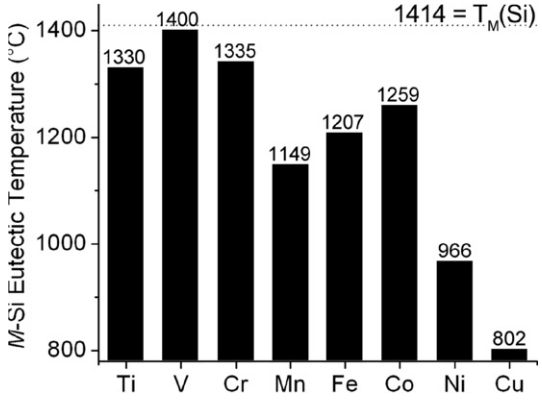

Fig. 5. Binary eutectic temperatures of Si and various 3d transition metal impurities, when cooling from the Si-rich side of the phase diagram. Note the extremely low eutectic point for Cu–Si, over 600 °C below the melting temperature of Si. Extracted from phase diagram data in [54].

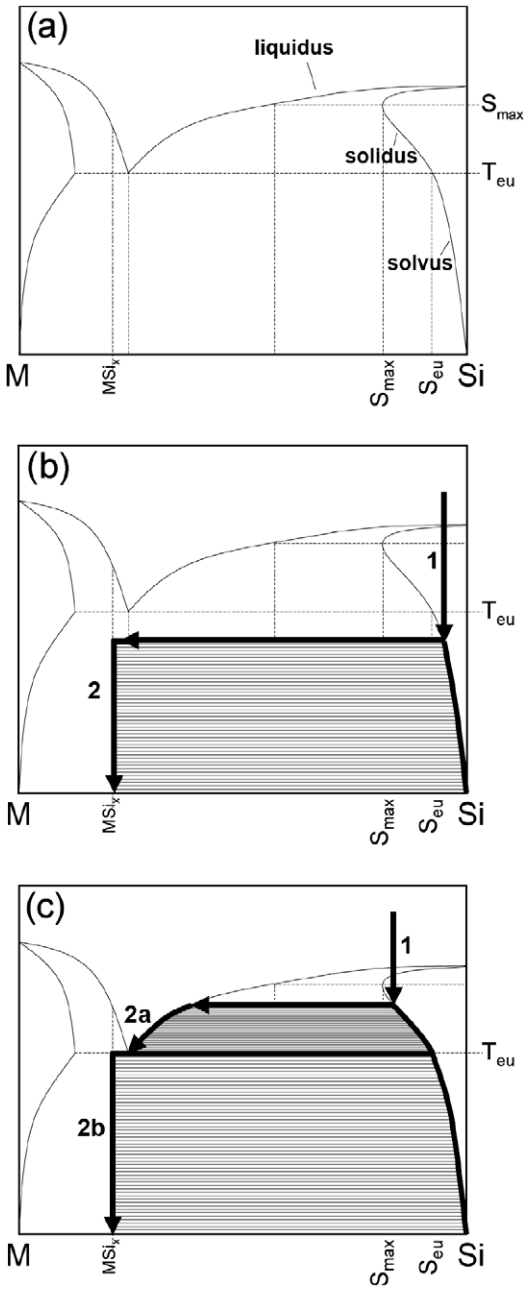

Fig. 6. (a) A generic 3d transition metal–silicon binary phase diagram, not dissimilar to Cu–Si. Note the point of maximum solid solubility of M in Si (S_{max}) occurs well above the eutectic temperature (T_{eu}), owing to a phenomenon known as 'retrograde solubility'. (b) Upon cooling (arrow 1), when the M concentration is below the solid solubility at the M–Si eutectic temperature, one expects M to precipitate into solid MSi_x precipitates (arrow 2), as shown by the arrows on the phase diagram. (c) However, when the M concentration is above the solid solubility at the M–Si eutectic temperature, the phase diagram predicts that M will precipitate and form liquid M–Si droplets, and then follow the liquidus towards the eutectic point (arrow 2a), resulting in the formation of solid precipitates below the eutectic temperature (arrow 2b).

a key role in ensuring a low melting temperature for a metal–silicon liquid, it appears from this and other experiments [42] that only a limited amount of Cu can be absorbed within the α-$NiSi_2$ host structure. It is conceivable that the Cu_3Si nodules consist of the remaining Cu

that, because of its finite solubility in the α-$NiSi_2$ structure and low Cu–Si eutectic point, was the last to solidify.

An additional distinguishing feature of precipitates formed as the result of high-temperature annealing is the extraordinarily large precipitate size—up to several microns in diameter in intentionally contaminated materials. While colonies of nano-precipitates can easily reach such dimensions (Fig. 1c, Refs. [8,38,43]), it is unusual to observe individual precipitates of these sizes, such as those in Fig. 3c (note the comparatively high count rate relative to Fig. 1, indicating a continuous particle as opposed to a colony of nano-precipitates). Even in samples intentionally contaminated at similar temperatures, precipitates of such sizes are rarely detected when only one impurity species is present, especially in the case of iron [10].

Assuming precipitate formation can indeed occur via an intermediary liquid system (droplet), one might speculate that other metals may accumulate within the liquid droplet via solid–liquid segregation. Many examples of metal accumulation via solid–liquid segregation exist in silicon-based systems; the simplest example occurs during silicon crystal growth from silicon-rich melt solutions, when metal impurities are rejected from the solid crystal into the melt (for a review, see [44] and references therein). More sophisticated examples include segregation of impurities to liquid M–Si eutectic layers on free surfaces (e.g., Al–Si [9,45,46], Zn–Si [47], Mn–Si [48], Au–Si [49], Pt–Si [49], Co–Si [49], Pb–Si [49], Sn–Si [49] and Ni–Si [47,49–52]) and segregation of metals to ion-implantation-induced Al–Si eutectic droplets within bulk Si [53]. The distinguishing feature of the mechanism proposed herein would be the formation of the gettering agent; i.e., precipitation of dissolved metallic impurities into liquid metal–Si droplets. One may even speculate that the embedded particle may remain liquid well below the equilibrium binary eutectic temperature, owing to the presence of other impurity species in multinary systems and, where appropriate, nano-scale size effects [41].

One could hypothesize that this precipitate formation mechanism, if properly understood, can be harnessed to improve the electronic quality of multicrystalline silicon wafers for solar cells. During multicrystalline silicon ingot growth, the formation of liquid droplets could serve to locally getter (via solid–liquid segregation) metallic impurities to the droplets, thus reducing the dissolved bulk concentrations of impurities elsewhere and increasing the overall material electrical quality. The power of this mechanism lies in the fact that metals are agglomerated by segregation into a liquid phase—an effective mechanism at elevated temperatures when most metals are highly mobile but not necessarily supersaturated. The magnitude of this effect on finished solar cell efficiency can be expected to vary, depending on the concentration and nature of the gettering agent intentionally added to the melt (e.g., Cu), the concentrations and natures of the native impurity species to be gettered (e.g., Fe, Ti), crystal growth conditions (e.g., time–temperature profile, planarity of the melt–solid interface), and the interaction of the as-grown impurity configuration with other gettering and high-temperature steps during solar cell processing. If properly harnessed, this phenomenon may be able to improve existing solar cell technology or extend the usable range of feedstock materials. It may also figure in the explanation of why certain impurity species with large nucleation energy barriers (e.g., Fe) precipitate readily in the presence of copper [10,55].

5. Summary and conclusions

By means of synchrotron-based X-ray microprobe techniques, the chemical states, sizes and nano-scale morphologies of precipitates formed in silicon contaminated with multiple-metal species were analyzed and subsequently annealed/cooled from two distinct temperature regimes: low (655 °C) and high (1200–1414 °C). The features of precipitates formed in these two temperature ranges differ substantially, and therefore it is proposed that different precipitate formation mechanisms are active in these two regimes.

Precipitates formed during annealing and cooling from low temperatures (655 °C) are easily explained by existing precipitation models and thermodynamic understanding. Metals are observed to precipitate into solid, equilibrium single-metal silicide phases, facilitated by lattice strain minimization or by the presence of defects, other metal precipitates, and/or favorable point defect concentrations. In single-crystalline silicon, Cu_3Si microcolony growth is observed, whereas no such colonies are observed at grain boundaries in mc-Si.

Features of precipitates formed during cooling from high temperatures ($\geqslant$1200 °C) are difficult to explain using classic precipitation models and are indicative of other precipitation mechanisms. Given the observed formation of mixed-metal silicide systems, nano-scale phase separation, relatively repeatable and homogeneous compositions, and large precipitate sizes, in addition to respective metal–silicon phase diagram information, it is proposed that these precipitates may have formed via a liquid–alloy intermediate phase. With liquid droplets within the Si bulk, it is plausible that precipitate ripening may have been enhanced by solid–liquid segregation of other metals; this hypothesis is substantiated by the absence of similarly large precipitates in samples contaminated only with a single metal species. These results and discussion reveal that the co-precipitation of multiple-metal species in silicon is a field ripe for further investigations, including formation mechanisms, electrical properties and dissolution kinetics, among others.

Acknowledgements

Many thanks to S.K. Estreicher, L. Felton, M. Seibt and P. Zhang for helpful discussions. One of the authors (M. Heuer) acknowledges the Deutsche Forschungsgemeinschaft for supporting project HE 3570/2-1. The Advanced Photon Source and the Advanced Light Source are supported by the Director, Office of Science, Office of Basic

Energy Sciences, of the US Department of Energy under Contract Nos. DE-AC02-06CH11357 and DE-AC02-05CH11231, respectively.

References

[1] Seibt M, Sattler A, Rudolf C, Voß O, Kveder V, Schröter W. Phys Status Solidi A 2006;203:696.
[2] Buonassisi T, Istratov AA, Marcus MA, Lai B, Cai Z, Heald SM, et al. Nat Mater 2005;4:676.
[3] Buonassisi T, Istratov AA, Pickett MD, Heuer M, Kalejs JP, Hahn G, et al. Prog Photovoltaics 2006;14:513.
[4] Istratov AA, Buonassisi T, McDonald RJ, Smith AR, Schindler R, Rand JA, et al. J Appl Phys 2003;94:6552.
[5] Macdonald D, Cuevas A, Kinomura A, Nakano Y, Geerligs LJ. J Appl Phys 2005;97:033523.
[6] Buonassisi T, Istratov AA, Heuer M, Marcus M, Jonczyk R, Isenberg J, et al. J Appl Phys 2005;97:074901.
[7] Solberg JK. Acta Crystallogr 1978;A34:684.
[8] Seibt M, Griess M, Istratov AA, Hedemann H, Sattler A, Schröter W. Phys Status Solidi A 1998;166:171.
[9] Buonassisi T, Marcus MA, Istratov AA, Heuer M, Ciszek TF, Lai B, et al. J Appl Phys 2005;97:063503.
[10] T. Buonassisi et al., submitted for publication.
[11] McHugo SA. Appl Phys Lett 1997;71:1984.
[12] Khalil RMENMB. Electrical properties of iron-doped silicon at different stages of precipitation. Ph.D. dissertation, Göttingen University, Göttingen, Germany; 2004.
[13] Jonczyk R, Rand JA, Grenko AJ, Moyer JG. In: Proceedings of the 19th European photovoltaic solar energy conference, Paris, France; 2004. p. 1263.
[14] Ryoo K, Drosd R, Wood W. J Appl Phys 1988;63:4440.
[15] Bolton JD, Youseffi M, Becker BS. Powder Metall 1998;41:93.
[16] Chaoli M, Ishihara S, Soejima H, Nishiyama N, Inoue A. Mater Trans 2004;45:1802.
[17] Longworth HP, Mikkola DE. Mater Sci Eng 1987;96:213.
[18] Marandel J, Schmitt B, Gantois M. Mem Sci Rev Metall 1973;70:731.
[19] Przybylowicz J, Kusinski J. Surf Coat Technol 2000;125:13.
[20] Kobelev NP, Soifer YM. J Phys IV 1996;6:811.
[21] Szeles C, Vertes A. Mater Sci Forum 1992;105–110:1265.
[22] Setton M. Ternary TM–TM–Si reactions. In: Maex K, van Rossum M, editors. Properties of Metal Silicides. London, UK: INSPEC; 1995. p. 129. ISBN 0-85296-859-0.
[23] Haider M, Sitter H. J Appl Phys 1987;62:3785.
[24] Czaputa R. Appl Phys A 1989;A49:431.
[25] Istratov AA, Hieslmair H, Weber ER. Appl Phys A 1999;69:13.
[26] Justo JF, Assali LVC. Int J Mod Phys B 1999;13:2387.
[27] Istratov AA, Buonassisi T, Marcus MA, Ciszek TF, Weber ER. In: Proceedings of the 14th NREL workshop on crystalline silicon solar cell materials and processes, Winter Park, USA; 2004. p. 165.
[28] Buonassisi T, Istratov AA, Marcus MA, Peters S, Ballif C, Heuer M, et al. In: Proceedings of the 31st IEEE photovoltaic specialists conference, Lake Buena Vista, USA; 2005. p. 1027.
[29] Heuer M, Buonassisi T, Marcus MA, Istratov AA, Pickett MD, Shibata T, et al. Phys Rev B 2006;73:235204.
[30] Ciszek TF, Wang TH. J Cryst Growth 2002;237–239:1685.
[31] Buonassisi T, Istratov AA, Peters S, Ballif C, Cai Z, Lai B, et al. Appl Phys Lett 2005;87:121918.
[32] Buonassisi T, Istratov AA, Marcus MA, Heuer M, Pickett MD, Lai B, et al. Solid State Phenom 2005;108–109:577.
[33] McHugo SA, Thompson AC, Flink C, Weber ER, Lamble G, Gunion B, et al. J Cryst Growth 2000;210:395.
[34] Yun W, Lai B, Cai Z, Maser J, Legini D, Gluskin E, et al. Rev Sci Instrum 1999;70:2238.
[35] Heald SM, Stern EA, Brewe D, Gordon RA, Crozier ED, Jiang D, et al. J Synchrotron Radiat 2001;8:342.
[36] Marcus MA, MacDowell AA, Celestre R, Domning E, Franck K, Manceau A, et al. J Synchrotron Radiat 2004;11:239.
[37] Seibt M, Hedemann H, Istratov AA, Riedel F, Sattler A, Schröter W. Phys Status Solidi A 1999;171:301.
[38] Nes E. Acta Metall 1974;22:81.
[39] Weber ER. Appl Phys A 1983;30:1.
[40] Dahmen U, Hagège S, Faudot F, Radetic T, Johnson E. Philos Mag 2004;84:2651.
[41] Xu Q, Sharp ID, Yuan CW, Yi DO, Liao CY, Glaeser AM, et al. Phys Rev Lett 2006;97:155701.
[42] Heuer M, Buonassisi T, Istratov AA, Pickett MD, Marcus MA, Minor AM, Weber ER. J Appl Phys 2007;101:123510.
[43] Nes E, Lunde G. J Appl Phys 1972;43:1835.
[44] Good EA. Impurity partitioning effects in silicon crystallization from metal: eutectic solutions for solar cell applications. Ph.D. dissertation, Colorado School of Mines, Golden, USA; 2004.
[45] Myers SM, Seibt M, Schröter W. J Appl Phys 2000;88:3795.
[46] Istratov AA, Hieslmair H, Weber ER. Appl Phys A 2000;70:489.
[47] Goetzberger A, Shockley W. J Appl Phys 1960;31:1821.
[48] Kulikov GS, Chichikalyuk YA, Yusupova SA. Fiz Tekh Poluprovodnikov 1995;29:469.
[49] Abdurakhmanov KP, Daliev KS, Kulikov GS, Lebedev AA, Utamuradova SB, Yusupova SA. Fiz Tekh Poluprovodnikov 1993;27:1222.
[50] Gay N, Martinuzzi S. Appl Phys Lett 1997;70:2568.
[51] Li J, Yang W-S, Tan TY, Chevacharoenkul S, Chapman R. Formation of a liquid metallic phase on silicon wafer surfaces during high temperature annealing. In: Bullis WM, Gosele U, Shimura F, editors. Defects in silicon II. Electrochemical Society; 1991. p. 651.
[52] Bemski G. Phys Rev 1956;103:567.
[53] Petersen GA, Myers SM. J Appl Phys 2001;89:4269.
[54] Predel B. Phase equilibria, crystallographic and thermodynamic data of binary alloys: electronic materials and semiconductors. Berlin, Germany: Springer; 1998, ISBN 3-540-61742-6.
[55] Macdonald D, Roth T, Geerligs LJ, Cuevas A. Solid State Phenom 2005;108–109:519.